Catalytic Hydrosilylation Routes to Divinylbenzene Bridged Silole and Silafluorene Polymers. Applications to Surface Imaging of Explosive Particulates

Jason C. Sanchez, Sara A. Urbas, Sarah J. Toal, Antonio G. DiPasquale, Arnold L. Rheingold, and William C. Trogler*

Department of Chemistry and Biochemistry, University of California at San Diego, 9500 Gilman Drive, La Jolla, California 92093-0358

Received October 12, 2007; Revised Manuscript Received December 14, 2007

ABSTRACT: The syntheses, spectroscopic characterization, and fluorescence quenching efficiencies of 1,1-silole− and 1,1-silafluorene−phenylenedivinylene polymers are reported. Model dimeric metallole compounds containing a phenylenedivinylene bridge have been synthesized to provide detailed structural and spectroscopic insight into conformational effects and electron delocalization. Poly((tetraphenyl)silole−phenylenedivinylene) and poly(silafluorene−phenylenedivinylene) both maintain a regioregular *trans*-vinylene Si−C backbone with $\sigma^*-\pi/\pi^*$ conjugation. Various hydrosilylation catalysts were screened to evaluate their ability to produce high molecular weight polymers and to direct a strictly *trans* product. Molecular weights (M_w) for these polymers are in the range of 8400−9600. Fluorescence spectroscopy shows a significant bathochromic shift for the silafluorene polymer from solution to the solid state. A surface detection method for the analysis of solid particulates of TNT, DNT, PA, RDX, HMX, Tetryl, TNG, and PETN by fluorescence quenching was explored. The blue-emitting silafluorene polymer exhibited improved sensitivity for detecting explosive particle residues as compared to previously reported metallole polymers. Detection limits as low as 100 pg cm^{-2} for TNT are obtained. The Stern−Volmer equation quantitatively models the fluorescence quenching of these polymers by TNT, RDX, and PETN in thin solid-state films.

Introduction

The recent rise in global terror threats and the general availability of high explosives and precursors thereof have increased demand for improved explosives screening processes. Current detection methods include but are not limited to gas chromatography coupled with mass spectrometry,[1] gas chromatography−electron capture detection,[2] surface-enhanced Raman spectroscopy,[3] mass spectrometry,[4] X-ray imaging, nuclear quadrupole resonance, thermal and fast neutron analysis, and ion mobility spectrometry,[5] colorimetric methods,[6] and fluorimetric detection.[7] The recent success of amplified fluorescence quenching with conjugated polymers to detect nitroaromatics[8] has prompted the development of new polymeric materials for explosives detection. Luminescent polymers offer rapid response times, low detection limits, intuitive interpretation, and cost-efficient solutions. The properties of luminescent polymers can be altered through tuning of the HOMO and LUMO energy levels through chemical modification of the polymer backbone and the degree of π-conjugation.[9] By extending the conjugation length, properties such as electron−hole mobility, emission wavelength, crystal packing (excimer emission), and amplified chemosensor response can be altered. Poly(*p*-phenyleneethynylene)s have been widely studied because of their highly rigid and delocalized structures. The use of acetylenic polymers can be problematic in solid-state applications due to self-quenching, so bulky pendent groups are required to prevent the π-stacking that leads to quenching; however, this often requires lengthy syntheses.

Another approach is to use a more flexible vinylene framework that maintains orbital conjugation while inhibiting π-stacking in thin-films. Polymers consisting of *p*-vinylene units are among the most popular due to their strong emissive properties.[10] Techniques used to access these vinylic functionalities include Heck coupling,[11] Wittig condensation,[12] the Gilch route,[13] and the Suzuki−Heck cascade.[14] These reactions either require multistep synthetic procedures, harsh reaction conditions, and specific precursors or are incompatible with various functional groups. To maximize conjugation, a regular trans-stereochemical framework is essential. A lack of regioregularity can shorten the length of the conjugated segments within the polymer and inhibit exciton mobility along the polymer backbone. Characterization of the stereochemistry of the important vinylene bridge is often difficult due to broadening in the aromatic region of the ^{1}H NMR spectrum of high molecular weight polymers.

Silane−phenylenedivinylene copolymers have recently been synthesized by hydrosilylation and palladium-catalyzed coupling of dihydridosilanes with unsaturated carbon linkers (Figure 1a).[15−18] These copolymers are slightly delocalized through $\sigma-\pi$ conjugation in the silicon−carbon framework. Silicon-doped poly(vinylenes) are also promising OLED and preceramic materials.[19−23] The inclusion of silicon into the polymer framework stabilizes the structure and creates a more flexible and soluble polymer.[24] Delocalization is limited in these polycarbosilanes because of minimal conjugation between π-systems through the silicon atom and the mixture of geometric isomers often produced during the hydrosilylation reaction (*trans*, *cis*, *gem*). These polymers also lack the visible photoluminescence (PL) properties required for imaging applications as fluorescent chemosensors.

Siloles, or 1-silacyclopentadienes, and poly(tetraphenyl)siloles have attracted attention because of their unique photoluminescent properties.[25,26] Applications include electron-transporting materials[27] and inorganic polymer sensors,[28−31] which take advantage of the $\sigma^*-\pi^*$ conjugation between the σ^* orbital on the silicon centers of the polymer backbone and the π^* molecular orbital of the butadiene moiety in the metallole ring.

10.1021/ma702274c CCC: $40.75
Published on Web 02/05/2008

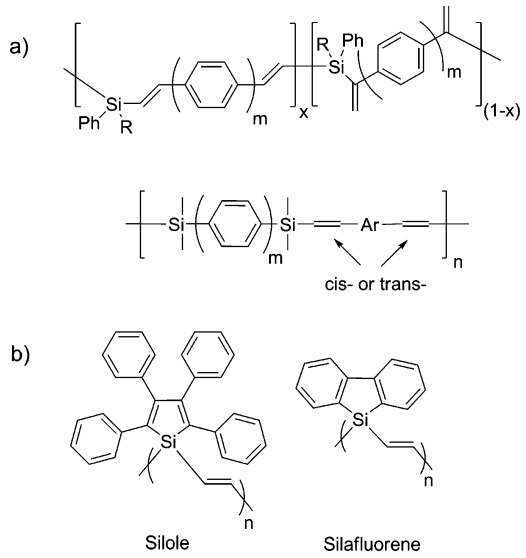

Figure 1. Chemical structures of silicon-containing vinylene polymers. (a) Silane−phenylenevinylene polymers with irregular stereochemistry about the vinylene moieties. (b) Silole− and silafluorene−vinylene polymers with $\sigma^*-\pi/\pi^*$ conjugation through the silicon center.

Scheme 1. Hydrosilylation of Trimethylsilylacetylene by 1-Hydrido-1-methyl-(tetraphenyl)silole Using H_2PtCl_6

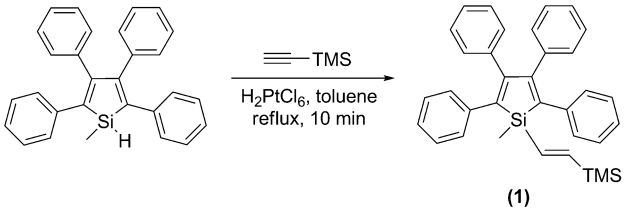

Dehydrocoupling[32] and Wurtz coupling[33] approaches have been used to prepare these materials, which are short chain oligomers that are susceptible to photobleaching from the weak Si−Si backbone. Hydrosilylation has also been used to create short polymer chain conjugated silole and silafluorene polymers that incorporate a vinylene-bridged Si−C backbone (Figure 1b).[34] These polymers have shown promise as a new class of robust, conjugated vinylene polymers for chemical sensor and UV-emitting applications. However, visualization of these polymers is not optimal due to their predominant UV-emission properties. Silafluorene is attractive as a fluorophore because of its ability to sense a wide range of explosive analytes.[34] It also provides improved thermal stability and eliminates g-band (green emission) defects often seen in fluorene-based UV-blue-emitting materials.[35] The copolymerization of silafluorene in the 1,1-positions with an unsaturated organic comonomer offers the possibility of a new type of stable blue-emitting material.

This paper focuses on the synthesis of silole and silafluorene copolymers by catalytic hydrosilylation of 1,4-diethylnylbenzene (DEB) for use in explosives detection. These materials form a new class of easily synthesized phenylene−divinylene conjugated polymers. Model dimeric complexes were synthesized and characterized by single-crystal X-ray diffraction to provide insight into the structural conformation and orbital overlap in these systems. Catalyst and reaction temperatures were varied to optimize formation of the regioregular *trans* product. The photoluminescence properties of these materials were characterized both in solution and in thin films. The blue-emitting silafluorene copolymer exhibits excellent detection for a wide range of common high explosives. The ease of synthesis, processability, and enhanced detection limits obtained for a range of explosives make them attractive alternatives to current

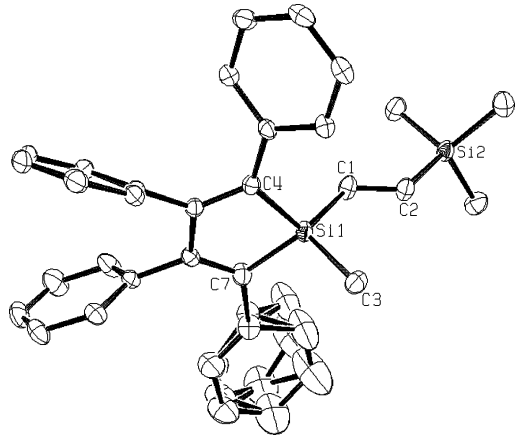

Figure 2. Thermal ellipsoid plot of **1** at the 50% probability level. Selected bond lengths (Å): Si1−C1 1.856(2), C1−C2 1.866(1), Si2−C2 1.358(2) and angles (deg): Si1−C1−C2 93.21(6), C1−C2−Si2 107.4(1), C3−Si1−C1 107.0(1), C4−Si1−C7 116.1(1). The phenyl ring bound to C7 was modeled with a disorder model using two conformations.

Scheme 2. Synthesis of 2 and 3 by Catalytic Hydrosilylation

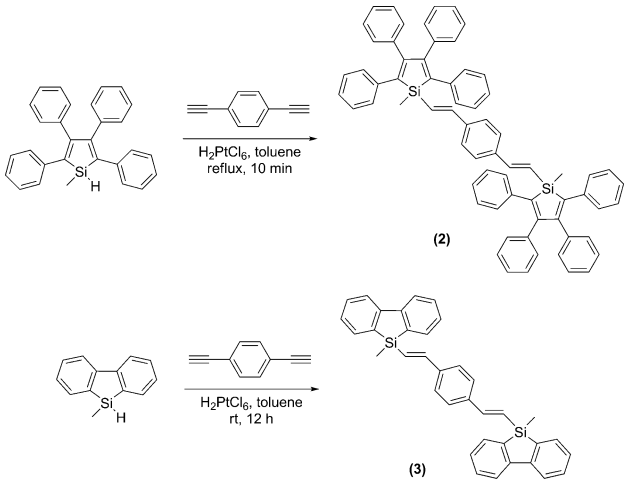

particle sensing technology. The thin-film stability, extended conjugation, and conformational flexibility also make these polymers promising new materials for blue-emitting photoluminescence and possibly electroluminescence applications.

Results and Discussion

To test whether hindered siloles would undergo catalytic hydrosilylation, 1-methyl-1-*trans*-(2-trimethylsilyl)ethenyl-2,3,4,5-(tetraphenyl)silole (**1**) was synthesized by the H_2PtCl_6 (CPA)-catalyzed hydrosilylation of trimethylsilylacetylene with 1-methyl-1-hydrido(tetraphenyl)silole (Scheme 1). The starting material is consumed within 10 min, as indicated by the disappearance of the Si−H proton resonance and appearance of vinylic protons in the ^{1}H NMR spectrum. The crystal structure reveals exclusive *cis*-β-addition (yielding the *trans* product) to the trimethylsilylacetylene group, which is promoted by steric crowding between the metalloid center and the 2,5-phenyl groups on the silole unit (Figure 2). With β-addition favored, this approach held promise for the stereospecific synthesis of regular copolymers by catalytic hydrosilylation.

Model dimeric complexes were then synthesized to aid structural characterization of new phenylenedivinylene polymers (Scheme 2). Synthesis of 1,4-di(1-methyl-1-*trans*-ethenyl-2,3,4,5-(tetraphenyl)silole)benzene (**2**) produced a regioregular structure using CPA catalyst in toluene at temperatures ranging

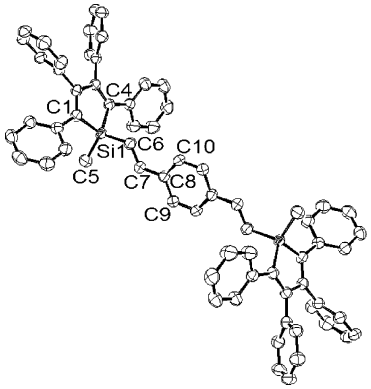

Figure 3. Thermal ellipsoid plot of **2** at the 50% probability level. Hydrogen atoms and solvent molecules omitted for clarity. Selected bond lengths (Å): Si1−C6 1.8461(18), C6−C7 1.325(2), C7−C8 1.473(2) and angles (deg): C1−Si1−C4 92.57(8), Si1−C6−C7 125.69-(15), C6−C7−C8 127.13(18).

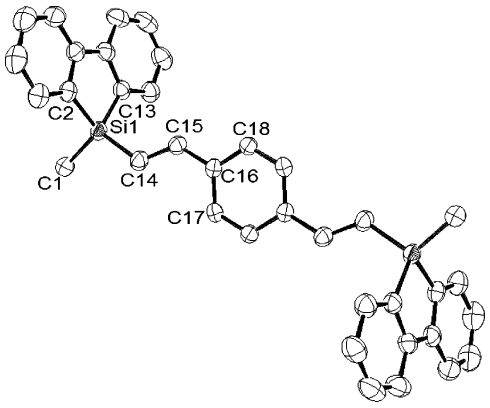

Figure 4. Thermal ellipsoid plot of **3** at the 50% probability level. Hydrogen atoms omitted for clarity. Selected bond lengths (Å): Si1−C14 1.848(2), C14−C15 1.337(3), C15−C16 1.476(3) and angles (deg): C2−Si1−C13 91.08(9), Si1−C14-C15 123.14(16), C14−C15−C16 126.13(18).

from 25 °C to its boiling point (Scheme 2). A strictly *trans* product was confirmed by X-ray diffraction (Figure 3). The synthesis of 1,4-di(1-methyl-1-*trans*-ethenyl-silafluorene)benzene (**3**) was first attempted by refluxing the starting materials in toluene; however, the ^{1}H NMR spectrum revealed a mixture of *cis* (doublet at 6.41 ppm, $J = 19$ Hz), *gem* (two doublets at 6.03 and 5.83 ppm, $J = 2.4$ and 2.4 Hz), and *trans*-vinyl (two doublets at 7.07 and 6.51 ppm, $J = 19.2$ and 19.2 Hz) isomeric products. However, by stirring the starting materials at room temperature for 12 h, the *trans*-only product **3** was obtained in 79% yield. X-ray quality crystals were obtained by slow evaporation of a hexane solution, and the structure was found to adopt a regioregular *trans* structure for both vinylene functionalities (Figure 4). The effect of reaction temperature on the stereochemistry of **3** is explained by the sterically less demanding environment at silicon for the silafluorene moiety as compared with the (tetraphenyl)silole. On oxidative addition to the platinum center, 1,2-insertion of the Si−H bond across the coordinated triple bond of DEB exhibits reduced steric control in the case of the silafluorene. Therefore, a reduced temperature is necessary to select the kinetically favored *trans* product.

To test the importance of steric crowding, we synthesized an iptycene-substituted silafluorene (Figure 5). The iptycene functionality provides a bulky framework around the silafluorene core unit. Attempts to polymerize this siliptycene monomer by both dehydrocoupling and catalytic hydrosilylation of 1,4-

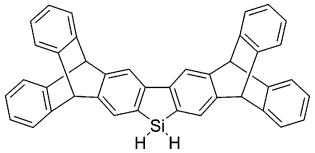

Figure 5. Chemical structure of 1,1-dihydrido-4,5,8,9-bis(triptycene)-silafluorene (siliptycene). The experimental procedure for its synthesis is provided in the Supporting Information.

diethynylbenzene failed over a range of temperatures and catalysts. The lack of reactivity observed at the silicon center supports the notion that catalytic hydrosilylation in these systems is susceptible to control by steric effects.

The *trans*-vinylene bond lengths of 1.325(2) Å in **2** are typical carbon−carbon bond lengths. The torsion angles for Si1−C6−C7 (silole−vinyl) and C6−C7−C8 (vinyl−phenyl) are 125.69-(15)° and 127.13(18)°, respectively. The out-of-plane angle between the vinylene groups and the bridging phenylene functionality is only 7.0°. However, the vinylene unit plane for **2** lies at 84.8° with respect to the face of the silole unit. This near-orthogonal alignment suggests minimal orbital overlap between the vinylene unit and the σ^* orbital of the silicon center. The poor alignment at the silicon center should reduce exciton delocalization along the chain in the polymer if a similar structure is adopted as for the dimer.

Dimer **3** shows a similar structure as **2** with a *trans*-vinylene bond length of 1.337(3) Å and torsion angles of 123.14(16)° and 126.13(18)° for Si1−C14−C15 (silafluorene−vinyl) and C14−C15−C16 (vinyl−phenyl), respectively. The torsion angles are slightly smaller than the ones observed in **2** due to the less sterically demanding silafluorene moiety. The out-of-plane angle between the vinylene groups and the bridging phenylene functionality is 20.9°. The plane of the vinylene unit in **3** is at 71.0° with respect to the plane of the silafluorene unit. This allows the π-orbitals of the vinylene unit to better face the silacyclopentadiene, creating partial overlap with the σ^* orbitals of the silicon center. Since the σ^* orbitals at silicon have a major contribution to the LUMO of this photoluminescent monomer, conjugation in the silafluorene polymers is expected to be better than in the (tetraphenyl)silole analogue. Figure 6 contains the superimposed structures of the dimers.

With the stereochemical regularity of the hydrosilylation reaction optimized through kinetic control, poly((tetraphenyl)-silole−phenylenedivinylene) (**4**) and poly(silafluorene−phenylenedivinylene) (**5**) were synthesized in good yield (>80%) with the CPA catalyst (Scheme 3). Isolated yields are lower than the spectroscopic yields due to the removal of low molecular weight oligomers through multiple precipitations. Although CPA is a commonly used heterogeneous catalyst for hydrosilylation reactions, several other catalysts were screened for the copolymerization of 1,1-dihydrido(tetraphenyl)silole (H_2-silole) and 1,1-dihydridosilafluorene (H_2SF) with DEB in an attempt to improve polymer yields and to increase molecular weights. The catalysts screened include Wilkinson's catalyst ($RhCl(PPh_3)_3$), $Pd(PPh_3)_4$, and Karstedt's catalyst (platinum−divinyltetramethyldisiloxane) (Table 1). All polymers were analyzed using ^{1}H NMR and GPC to characterize polymer stereoregularity and molecular weights, respectively. Although the $Pd(PPh_3)_4$ catalyst forms **4** and **5** in high yields, and with comparable molecular weights (Table 1), the removal of the homogeneous catalyst presents a purification challenge. Wilkinson's catalyst produces slightly lower molecular weights with lower yields. This could be due to competitive polymerization pathways as it is also an effective catalyst for dehydrocoupling.[32] Karstedt's catalyst produces the lowest molecular weights and

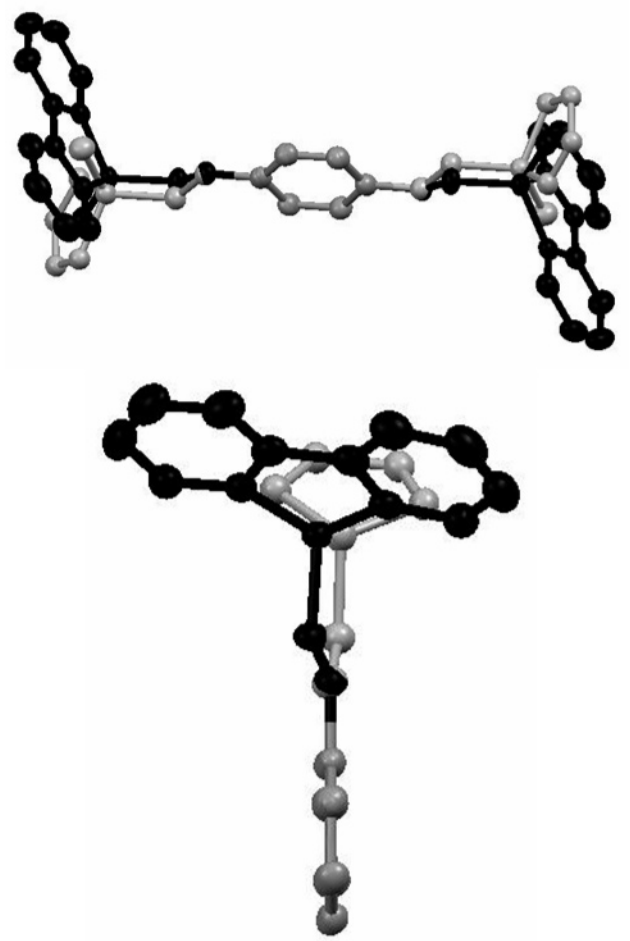

Figure 6. Superimposed crystal structures of **2** (gray atoms) and **3** (black atoms). Structures were aligned according to the phenylene subunit. Top: a side view of the structures. Hydrogen atoms and phenyl rings for **2** were omitted for clarity. Bottom: a view down the plane of the phenylene ring with half of the structures omitted for clarity. The large out-of-plane angle for **3** as compared to **2** allows for better orbital overlap between the vinylene group (π/π^*) and the silicon center (σ^*).

Scheme 3. Synthesis of 4 and 5 by Catalytic Hydrosilylation

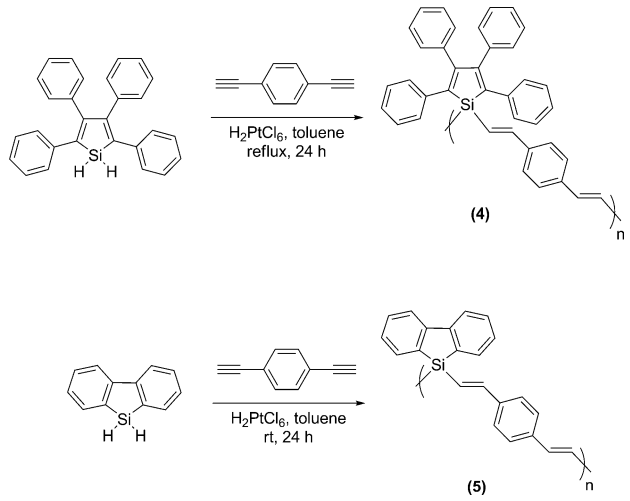

yields of the four catalysts studied. This liquid platinum disiloxane catalyst is inconvenient and separation from the product is problematic. Overall, CPA produces the highest molecular weights and yields, and it is separated easily from the polymer by filtration. Polymers $\mathbf{4_a}$ and $\mathbf{5_a}$ seen in Table 1 were chosen for all the photoluminescence and explosives

Table 1. Polymerization Results for 4 and 5 Prepared by Catalytic Hydrosilylation with Various Catalysts in Toluene for 24 h

entry	conditions	catalyst[a]	yield[b] (%)	M_w (GPC)	M_w/M_n[c]
$\mathbf{4_a}$	reflux	H_2PtCl_6	51	8400	1.8
$\mathbf{4_b}$	reflux	Wilkinson's catalyst	49	6000	1.8
$\mathbf{4_c}$	reflux	Karstedt's catalyst	67	5600	1.5
$\mathbf{4_d}$	reflux	$Pd(PPh_3)_4$	75	5500	1.3
$\mathbf{5_a}$	room temp	H_2PtCl_6	68	9600	2.0
$\mathbf{5_b}$	room temp	Wilkinson's catalyst	63	4400	1.7
$\mathbf{5_c}$	room temp	Karstedt's catalyst	69	3700	2.1
$\mathbf{5_d}$	room temp	$Pd(PPh_3)_4$	51	5300	1.8

[a] Reactions performed with following quantity of catalyst (mol %): H_2PtCl_6 (0.2), Wilkinson's (2.0), Karstedt's (1.0), $Pd(PPh_3)_4$ (1.0). [b] Calculated after three precipitations from methanol. [c] Calculated by GPC.

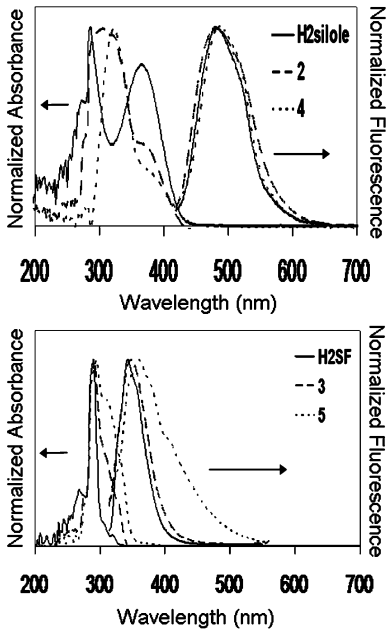

Figure 7. UV−vis and fluorescence spectra of siloles (H_2silole, **2**, and **4**) and silafluorenes (H_2SF, **3**, and **5**) showing a bathochromic emission shift for the polymers, and peak broadening of **5**.

detection studies and will hereafter be referred to as **4** and **5**, respectively.

Photoluminescence. Photoluminescence (PL) data for all the compounds synthesized in this study are listed in Table 2. For the silole-containing materials, there is no shift in the fluorescence emission from monomer (H_2silole) to dimer **2** (Figure 7). There is only a slight bathochromic shift of 5 nm (213 cm^{-1}) for the corresponding polymer **4**. These results are consistent with the structural analysis, which revealed an orthogonal alignment of the bridging organic π-system and the Si−C σ^*-orbitals in dimer **2**. The flexibility of the phenylene-divinylene units in solution for high molecular weight materials, such as polymer **4**, may allow population in the solution phase of some conformers with improved alignment. In contrast, the silafluorene dimer revealed a better alignment for conjugation of the bridging organic π-system and the Si−C σ^*-orbitals. The fluorescence emission of dimer **3** is red-shifted 5 nm (419 cm^{-1}) from the H_2SF monomer (Figure 7), and polymer **5** is red-shifted another 11 nm (880 cm^{-1}) from dimer **3**. There is also significant peak broadening in the emission spectrum of polymer **5** as compared to H_2SF and **3**. This suggests that polymer **5** has a partially delocalized structure and is a better candidate for fluorescence detection applications with improved exciton mobility.

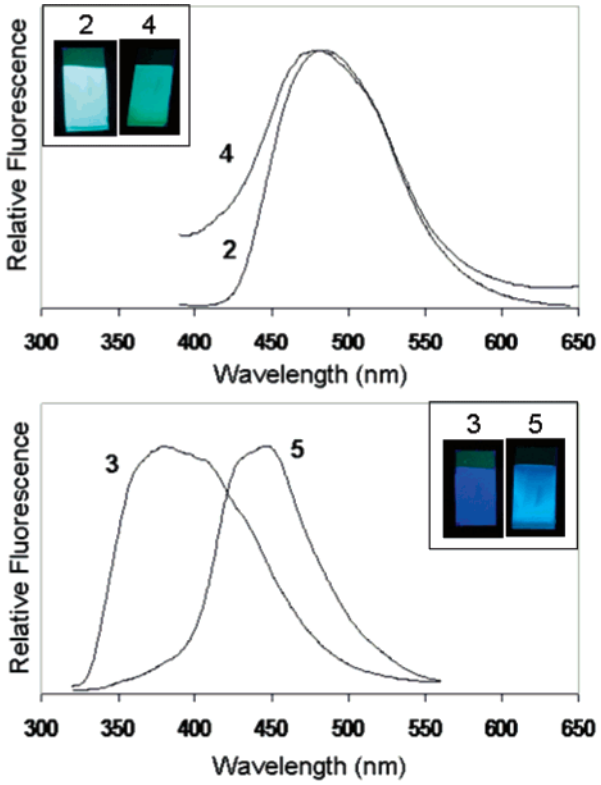

Figure 8. Solid-state fluorescence emission spectra for siloles (**2** and **4**) and silafluorenes (**3** and **5**). Inserted figures depict the luminescence observed under a UV lamp (302 nm) for thin films of **2**−**5** on silica TLC plates.

Quantum yield measurements show that the silafluorene materials are efficient emitters in solution. Polymer **5** has a fluorescence quantum yield of ∼4%, which is an order of magnitude greater than polymer **4**. However, polymer **4** has a higher solution fluorescence quantum yield than previously prepared (tetraphenyl)silole polymers.[32] Conformational flexibility in solution is known to increase nonradiative decay pathways, lowering the fluorescence quantum yields in solution as compared to the solid state.[36] Thus, the rigid siliptycene monomer (Figure 5) has the highest solution emission quantum yield (27%). It is well-known that solid-state emission intensities of the (tetraphenyl)silole polymers are often 20−30 times larger than in solution, an effect called aggregation-induced emission (attributed to restricted phenyl ring rotation in the solid state).

Solid-state fluorescence studies were conducted to gain insight into the thin-film PL properties of polymers **4** and **5**. Previous studies with (tetraphenyl)silole and silafluorene-containing polymers show that silica thin-layer chromatography (TLC) plates serve as an effective, low-cost medium for the analysis of thin-film PL properties.[34,37] Polymers **4** and **5** were developed onto silica TLC plates (Whatman PE SIL G/UV) using chloroform (4 mg mL^{-1}). The area developed was maintained at 6 cm^2 for each sample. Dimers **2** and **3** were examined for comparison. Figure 8 shows the fluorescence emission comparison between dimers and polymers in the thin films. Polymer **4** shows no significant shift in the emission spectrum from its dimer **2** or from its solution-phase emission (Figure 7). This supports the conclusion that there is limited conjugation through the backbone of this polymer and that the sterically demanding phenyl substituents prevent interchain stacking and excimer emission.[37] In contrast, the thin-film fluorescence spectrum for polymer **5** is shifted 88 nm (5484 cm^{-1}) from its solution-phase emission spectrum. This is consistent with formation of a partially ordered film where π-stacking interactions between polymer chains create a network of overlapping frontier molecular orbitals, facilitating excimer emission. There is a change from a predominantly high-energy UV emission in solution to a blue emission in solid films. This dramatic red-shifted luminescence is an important feature for solid-state emitting applications and improves visualization of the polymer film for imaging sensor applications.

Explosives Detection. Important high explosives for fluorescence quenching detection applications contain nitroaromatic, nitrate ester, or nitramine functionalities.[38] Fluorescence detection takes advantage of the relatively low LUMO energies of these explosive materials, which can accept an excited-state electron from the fluorophore. Fluorescence detection studies were carried out with a range of explosives materials including 2,4,6-trinitrotoluene (TNT), picric acid (PA), 2,4-dinitrotoluene (DNT), cyclotrimethylenetrinitramine (RDX), cyclotetramethylene−tetranitramine (HMX), 2,4,6-trinitrophenyl-*N*-methylnitramine (Tetryl), trinitroglycerin (TNG), and pentaerythritol tetranitrate (PETN). Detection of explosive particulates and solid film residues were a focus, rather than detection of vapors, since the explosives studied have very low vapor pressures. Vapor pressures of production-line explosive mixtures can be further reduced by a factor 1000 when sealed in plastics.[38a] The method explored here focuses on visual imaging of trace explosive particles through a fluorescence quenching process.

Previous investigations using DFT calculations have shown that explosive analytes have a large range of LUMO energies, rendering it difficult to detect the broad class with one fluorescent sensor.[34] We recently have had success using UV-emitting silafluorene materials that incorporate a high-energy ^{1}SOMO (singlet singly occupied donor molecular orbital) that lies above the LUMO energy of a larger range of explosives than for previous fluorescence sensors.[34] However, visualization of these predominantly UV-emitting polymer films was difficult due to the low emission intensity in the visible region of the spectrum. Polymer **5** was designed to maintain a high-energy ^{1}SOMO with a slightly lower energy band gap for enhanced visible blue emission and easier visualization. Dilute standards of each explosive were prepared in toluene and stored in amber vials to prevent photodegredation. The explosive solutions were spotted onto Whatman filter paper or a porcelain tray at the desired concentration level with use of a glass microsyringe. Two surfaces were examined to determine any effect of substrate porosity on the explosive detection process. A solvent blank was included next to each analyte as a control. All solution spots were a 5 μL volume, producing a spot of ∼1 cm in diameter. After solvent evaporation, the substrate was airbrushed with a solution of polymer (0.5 mg of polymer mL^{-1} in 2:1 toluene: acetone) at a rate of 0.5 mL s^{-1}. The addition of toluene facilitates dissolution of explosive analytes for effective mixing with the polymers to form a solid solution on drying. Polymers **4** and **5** were visualized using a UV-B (λ_{em} = 302 nm) light source with a UV-transmitting filter to eliminate background radiation. Polymer **4** exhibits a yellow-green luminescence, and polymer **5** emits a bright blue luminescence. To verify that detection also worked for authentic bulk commercial explosives, a series of thumbprints containing production-line PETN (NEWTEC Services Group Inc.) were also examined, so the resultant contamination resembles what one may encounter in the field.

For visual assessment, a double-blind test was carried out using two spots of the explosive material at each concentration, spotted randomly onto three locations along with solvent blanks.

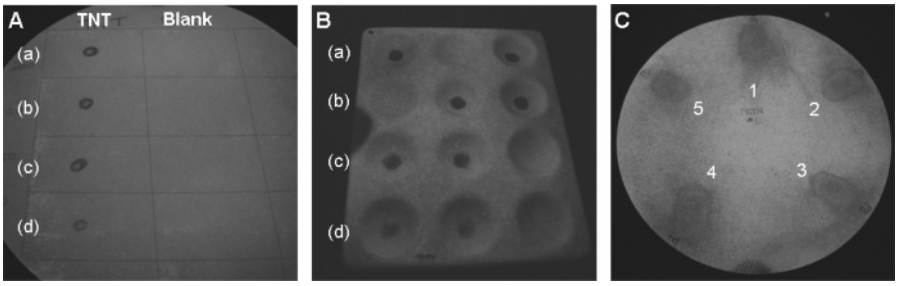

Figure 9. Examples of fluorescence quenching of a thin film of polymer **5** by solid particulates of various explosives imaged with a Sony 2.0 megapixel digital camera under continuous UV excitation (302 nm). (A) Detection of TNT particulates (a) 64, (b) 32, (c) 16, and (d) 3 ng cm^{-2} on filter paper. A toluene blank was spotted as a control. (B) Detection of tetryl particulates (a) 64, (b) 32, (c) 16, and (d) 3 ng cm^{-2} on a porcelain tray. The analyte was randomly place in 2 of 3 wells, and observed quenching was confirmed by an independent observer. (C) Detection of five successive thumbprints on filter paper contaminated with production-line PETN particulates. Successive prints were placed in succession without further handling of the explosive material.

Table 2. Summary of Photoluminescence Data for Monomers, Dimers, and Polymers

entry	λ_{abs} (nm)[a]	ϵ_{max} (L mol^{-1} cm^{-1})	solution λ_{flu} (nm)[a]	thin-film λ_{flu} (nm)[c]	Φ_{flu} (%)[d]
H_2silole	305	7500	482	485	0.13
H_2SF	288	7700	343	365	24
2	306	14000	482	482	0.65
3	290	31000	348	380	17
4	322	7600[b]	487	478	0.60
5	294	14000[b]	359	447	4.0

[a] UV−vis and fluorescence taken in toluene. [b] Absorptivities are calculated per mole of silicon. [c] Emission maximum for thin layer of fluorophore absorbed onto TLC plate. [d] Quantum yield (Φ_{flu}) of fluorescence ±30%, relative to 9,10-diphenylanthracene in toluene.

Illuminated samples were examined in a double-blind process by an independent observer, who judged when quenching was discernible. Dark spots in the luminescent film indicate quenching of the polymer by the analyte (Figure 9). Detection limits are reported as the lowest amount of explosive necessary for the independent observer to discern quenching visually and accurately (>95% accuracy) in the correct locations. A summary of the detection limits is provided in Table 3. Lower detection limits for polymer **4** were obtained on the smooth porcelain substrate as compared with the porous filter paper. However, polymer **4** is only able to detect the nitroaromatic explosives TNT, DNT, PA, and Tetryl. This is expected due to the unfavorable energy matching between the green-emitting (tetraphenyl)silole materials and the nonaromatic explosives with high-energy LUMOs.[34] Polymer **5** shows better detection limits for the nitroaromatic explosives than polymer **4**. The improved conjugation of **5** over **4** may play a role in the increased exciton migration and the amplified fluorescence quenching effect. Polymer **5** also shows the ability to detect the entire range of nitramine, nitroaromatic, and nitrate ester explosives studied at the same or better detection limits than achieved with previous polymers.[34,39] Several factors play a role in these results. Polymer **5** is highly luminescent in the visible blue region of the spectrum when placed in thin films. The spacing between silafluorene units in this phenylene−divinylene polymer is also greater than in the vinylene polymers, allowing room for better analyte-to-polymer interactions (Figure 10). These binding interactions take place at the Lewis acidic silicon center; therefore, less steric encumbrance surrounding these centers can lead to better detection limits.[34]

Surface detection of explosives particulates is inherently difficult to quantify. The human eye detection approach provides a practical, but qualitative, forensic test. To better quantify quenching efficiency at the molecular level, Stern−Volmer quenching constants were determined for solid-state detection. Silica TLC plates were chosen as the substrate due to the consistency and reliability of the thin-film PL results. This method offers a good imitation of a porous sampling substrate, such as filter paper, often used for the collection of unknown particulates. The analytes chosen for this solid-state study include TNT, RDX, and PETN, each representing a different class of nitrogen-based explosives. Solutions containing a dissolved explosive and either polymer **4** or **5** (4 mg mL^{-1} in $CHCl_3$) were individually developed onto the TLC plate with varying explosive concentrations. This creates a thin-film solid solution of polymer containing uniformly distributed explosive analytes. While the Stern−Volmer equation is usually applied to model a diffusing emitter and quencher, it also applies to

Table 3. Summary of Solid-State Detection Limits (ng cm^{-2}) for Various Explosives by Fluorescence Quenching of Polymers 4 and 5[a]

Explosive	Structure	P_{vap} (Torr)	4		5	
			Porcelain	Filter Paper	Porcelain	Filter Paper
TNT	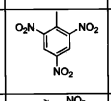	5.8×10^{-6}	3	6	0.1	0.1
Tetryl	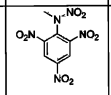	5.7×10^{-9}	1	1	0.1	0.2
DNT	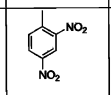	1.1×10^{-4}	6	13	0.6	0.3
PA	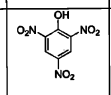	5.8×10^{-9}	1	1	2	0.3
PETN	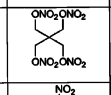	1.4×10^{-8}	—	—	0.6	1
RDX	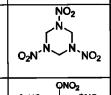	4.6×10^{-9}	—	—	3	2
TNG	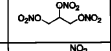	4.4×10^{-4}	—	—	6	2
HMX	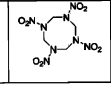	8.0×10^{-11}	—	—	6	3

[a] Dashed lines represent no detection at 64 ng cm^{-2} or less.

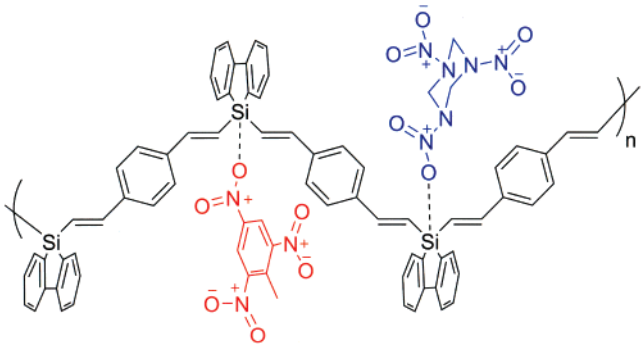

Figure 10. Schematic representation of explosive analyte binding events with polymer **5**. Planar aromatic molecules such as TNT (red) as well as aliphatic explosive molecules such as RDX (blue) can readily access the silicon centers by Lewis acid/base interactions in part due to the spacing between silicon units created by the phenylene−divinylene framework.

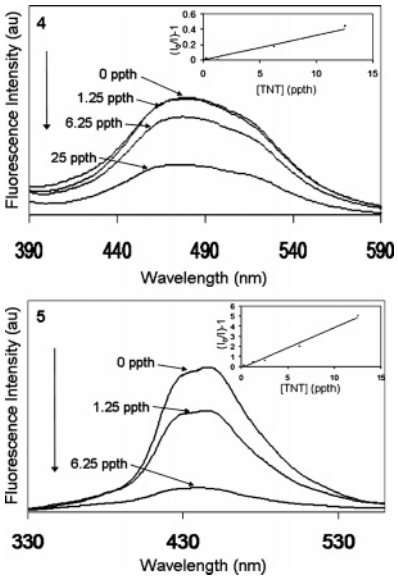

Figure 11. Solid-state fluorescence quenching of **4** (top) and **5** (bottom) by TNT on silica TLC plates. The concentration of explosive is reported in ppth of explosive-to-polymer (ppth = parts per thousand by weight). The inset in the upper right of each plot represents the linear regression analysis of the Stern−Volmer equation.

static quenching where the emitting species binds the quencher. The latter situation effectively applies in a solid solution. Another quantitative technique to measure the efficiency of a static fluorescence quenching process is the Perrin formulation. However, this method requires the measurement of absolute fluorescence quantum efficiencies in the bound and unbound state. These quantities are difficult to obtain for solid-state, thin-film analyses due to the lack of reliable reference materials. Therefore, the Perrin formulation is usually applied to highly concentrated solutions where the donor and acceptor moieties are covalently linked. To our knowledge, the Stern−Volmer analysis has not been used previously to model quenching efficiencies in solid solutions. A typical graph of the fluorescence from each film is provided in Figure 11, showing increasingly reduced emission in films containing increasing amounts of explosives. By plotting the change in fluorescence intensity vs the concentration of analyte in the solid solution, the Stern−Volmer constant is obtained for solid-state quenching from the slope of the line.

The observed quenching by TNT, RDX, and PETN reveals good agreement with the Stern−Volmer equation with R^2 values >0.98. A summary of the Stern−Volmer constants (K_{SV}) is given in Table 4. As expected, TNT is detected by both **4** and **5** with K_{SV} of 3.5×10^{-2} and 4.0×10^{-1} ppth^{-1} (ppth = parts per thousand by weight of the explosive dissolved in the polymer film), respectively. Since as little as 6 ppth of explosive can quench about 90% of the emission in polymer **5**, exciton delocalization (both inter- and intrapolymer chain) in the solid state must be significant. Polymer **4** failed to demonstrate fluorescence quenching in the presence of either RDX or PETN, consistent with the results from filter paper and porcelain solid-state detection studies. The fluorescence from polymer **5** is quenched in the presence of both PETN and RDX. However, the K_{SV} for these nonaromatic explosives are an order of magnitude lower than observed for TNT, similar to the visual filter paper and porcelain solid-state detection studies. Thus, the process of depositing solid solution films by evaporation of solutions of both analyte and fluorophore proved to be a simple and advantageous method of quantifying quenching efficiencies in the solid state. It also suggests possible algorithms for the estimation of explosive particles from the spray-on imaging method.

Table 4. Summary of Solid-State Stern−Volmer Constants (K_{SV}) for the Fluorescence Quenching of Polymers 4 and 5 by TNT, RDX, and PETN on Silica TLC Plates[a]

	K_{SV} (ppth^{-1})	
explosive	**4**	**5**
TNT	3.5×10^{-2}	4.0×10^{-1}
RDX		5.6×10^{-2}
PETN		5.0×10^{-2}

[a] Values reported in ppth^{-1} (ppth = parts per thousand by weight of the explosive dissolved in the polymer film). No quenching was observed for polymer **4** with RDX and PETN.

Insensitivity to common interferents is another important consideration when developing an explosive sensing polymer. Interference arises when fluorescence quenching results from a substance other than the targeted analyte. Polymers **4** and **5** show no change in luminescence when the polymer films are exposed to common organic solvents such as THF, toluene, benzene, acetonitrile, acetone, and methanol. There is some interference from spotted benzophenone and benzoquinone, but only at quantities exceeding 16 ng cm^{-2}. These oxidizing aromatic organic molecules, though not typically found in nature, are typical interferents for other fluorescence quenching polymers.[40]

Overall, detection of the targeted explosive analytes was achieved with excellent sensitivity. The strained silacycle of both the (tetraphenyl)silole and silafluorene comonomers act as Lewis acid centers that promotes binding of nitro- and nitrate-containing explosive analytes.[34] The incorporation of flexible phenylene−divinylene units prevents self-quenching processes in the thin films and maintains delocalization for fluorescence quenching. Polymer **5** shows a large bathochromic shift in the solid state, creating a bright blue emission at low surface concentrations. These new conjugated polymers show promise as stable and efficient fluorescing materials for chemosensor, photoluminescent, and possibly electroluminescent applications.

Experimental Section

General. *Caution: TNT and picric acid are high explosives and should be handled only in small quantities. Picric acid also forms shock sensitive compounds with heavy metals. Purchased explosive standards were handled as dilute solutions to eliminate their explosion hazard.* All synthetic manipulations were carried out under an atmosphere of dry argon gas using standard Schlenk techniques. Dry solvents were purchased from Aldrich Chemical Co. Inc. and used after purification with an MBraun Auto Solvent

Table 5. Summary of X-ray Crystallographic Data

	1	2	3
formula	$C_{34}H_{34}Si_2$	$C_{92}H_{78}Si_2$	$C_{36}H_{30}Si_2$
formula weight	498.81	1239.72	518.78
space group	$P2_1/n$	P-1	$Pbca$
a, Å	6.0014(4)	11.500(3)	14.3625(12)
b, Å	15.5685(11)	13.326(3)	13.0470(11)
c, Å	30.818(2)	13.958(3)	15.3108(13)
α, deg	90	62.081(4)	90
β, deg	93.6220(10)	74.553(4)	90
γ, deg	90	72.412(4)	90
V, Å^3	2873.6(3)	1781.7(7)	2869.1(4)
Z	4	1	4
crystal color, habit	colorless, block	yellow, block	colorless, prism
ρ(calc), g cm^{-3}	1.153	1.155	1.201
μ(Mo Kα), mm^{-1}	0.144	0.097	0.147
temp, K	100(2)	203(2)	203(2)
reflections measured	24 815	12 819	7100
reflections ind.	6505 [$R_{int} = 0.0269$]	8187 [$R_{int} = 0.0252$]	3288 [$R_{int} = 0.0336$]
$R(F)$ ($I > 2\sigma(I)$)[a]	0.0493	0.0596	0.0524
$R(wF^2)$ ($I > 2\sigma(I)$)[b]	0.1310	0.1563	0.1350

[a] $R = \sum||F_o| - |F_c||/\sum|F_o|$. [b] $R(\omega F^2) = \{\sum[\omega(F_o^2 - F_c^2)^2]/\sum[\omega(F_o^2)^2]\}^{1/2}$; $\omega = 1/[\sigma^2(F_o^2) + (aP)^2 + bP]$, $P = [2F_c^2 + \max(F_o,0)]/3$.

Purification System. Spectroscopic grade toluene from Fisher Scientific was used for the fluorescence measurements. Trimethylsilylacetylene and 1,4-diethynylbenezene (97%) were purchased from Aldrich Chemical Co. Inc. 1,4-Diethynylbenzene was sublimed before use (30 °C at 0.5 Torr). The following were prepared by literature methods: 1-hydrido-1-methyl(tetraphenyl)silole,[41] 1,1-dihydrido(tetraphenyl)silole,[32] 1-hydrido-1-methylsilafluorene,[42] and 1,1-dihydridosilafluorene.[43] NMR data were taken on 300, 400, and 500 MHz spectrometers. UV−vis spectra were obtained with the use of a Hewlett-Packard 8452A diode array spectrometer. A Perkin-Elmer LS 45 luminescence spectrometer was used to recorded fluorescence emission and excitation spectra. IR spectra were obtained on a Nicolet Magna-IR 550 spectrometer. GPC data were obtained with the use of a Viscotek GPCmax VE 2001 GPC; molecular weights were recorded relative to polystyrene standards and low molecular weight silole monomers and dimers.

X-ray Crystal Structure Determinations. Diffraction intensity data were collected with a Bruker P4/CCD Smart Apex CCD diffractometer at 100 K for **1** and 203 K for **2** and **3**. Crystal, data collection, and refinement parameters are given in Table 5. The space groups were chosen on the basis of systematic absences. The structures were solved by direct methods, completed by subsequent difference Fourier syntheses, and refined by full matrix least-squares procedures on F^2. The data were integrated using the Bruker SAINT software program and scaled using the SADABS software program. Solution by direct methods (SIR-2004) produced a complete heavy-atom phasing model consistent with the proposed structure. All non-hydrogen atoms were refined anisotropically by full-matrix least-squares (SHELXL-97). All hydrogen atoms were placed using a riding model. Their positions were constrained relative to their parent atom using the appropriate HFIX command in SHELXL-97. All software and sources of scattering factors are contained in the SHELXTL (5.10) program package (G. Sheldrick, Bruker XRD, Madison, WI).

1-Methyl-1-*trans*-(2-trimethylsilyl)ethenyl-2,3,4,5-(tetraphenyl)silole (1). 1-Hydrido-1-methyl(tetraphenyl)silole (500 mg, 1.25 mmol), trimethylsilylacetylene (1 mL, 7 mmol), and 0.1−0.5 mol % H_2PtCl_6 were vigorously refluxed in toluene (5 mL), under argon for 10 min. The dark orange solution was filtered through a sintered glass frit and evaporated to dryness. The remaining solid was dissolved in 1 mL of THF and precipitated with 10 mL of methanol, and the yellow powder was obtained by vacuum filtration on a sintered glass frit. The product was recrystallized from hot pentane, yielding yellow crystals (0.43 g, 68%). ^{1}H NMR (400.053 MHz, $CDCl_3$): δ 6.71−7.09 (m, 22H, silole Ph, and =CH−Si), 0.55 (s, 3H, CH_3), 0.065 (s, 9H, CH_3−Si). ^{13}C{^{1}H} NMR (100.59 MHz, $CDCl_3$): δ 157.4, 143.0 (t, =CH−Si), 154.9, 140.3, 139.6, 138.9 (q, carbons on silole ring and Ph), 130.0, 129.0, 127.8, 127.43, 126.2, 125.5 (q, Ph), −1.1 (s, $(CH_3)_3$-Si), −6.2 (s, CH_3). ^{29}Si{^{1}H} NMR (99.37 MHz, INEPT, $CDCl_3$, TMS (δ 0.00)): δ −2.96, −7.33. UV: λ_{abs} = 286, 366 nm. Fluorescence: λ_{em} = 478 nm, at λ_{ex} = 360 nm; mp = 118−119 °C. Calcd for $C_{34}H_{34}Si_2$: C 81.8, H 6.87. Found: C 81.2, H 6.95.

1,4-Di(1-methyl-1-*trans*-ethenyl-2,3,4,5-(tetraphenyl)silole)-benzene (2). 1-Hydrido-1-methyl(tetraphenyl)silole (500 mg, 2.6 mmol), 1,4-diethynylbenezene (170 mg, 1.3 mmol), and 0.1−0.5 mol % H_2PtCl_6 were vigorously refluxed in toluene (10 mL), under argon for 10 min. The dark orange solution was filtered through a sintered glass frit and evaporated to dryness. The remaining solid was dissolved in 1 mL of THF and precipitated with 10 mL of methanol, and the yellow powder was obtained by filtration on a sintered glass frit. The product was recrystallized from hot benzene, yielding yellow crystals (0.26 g, 72%). ^{1}H NMR (400.053 MHz, $CDCl_3$): δ 7.40 (s, 4H, benzyl), 6.83−7.10 (m, 42H, silole Ph, and =CH−Si), 6.64 (dd, 2H, =CH−Ph), 0.65 (s, 6H, CH_3). ^{13}C-{^{1}H} NMR (100.59 MHz, $CDCl_3$): δ 155.1, 147.4, 140.1, 139.5, 138.8, 138.1, 129.9, 129.0, 127.9, 127.5, 126.9, 126.3, 125.7, 122.8, −5.5. ^{29}Si{^{1}H} NMR (99.37 MHz, INEPT, $CDCl_3$, TMS (δ 0.00)) δ −1.40. Calcd for $C_{68}H_{54}Si_2$: C 88.1, H 5.87. Found: C 87.7, H 6.89.

1,4-Di(1-methyl-1-*trans*-ethenyl-silafluorene)benzene (3). 1-Hydrido-1-methylsilafluorene (311 mg, 1.6 mmol), 1,4-diethynylbenezene (311 mg, 0.8 mmol), and 0.1−0.5 mol % H_2PtCl_6 were stirred in toluene (5 mL) at room temperature, under argon for 12 h. The light yellow solution was passed through a sintered glass frit and evaporated to dryness. The remaining solid was purified by flash chromatography on silica gel using hexanes−dichloromethane as the eluent. Colorless crystals were collected from hexanes (0.325 g, 79%). ^{1}H NMR (400.053 MHz, $CDCl_3$): δ 7.86 (d, 4H, silafluorene−Ph), 7.57 (d, 4H, silafluorene−Ph), 7.44 (t, 4H, silafluorene−Ph), 7.36 (s, 4H, Ph), 7.29 (t, 4H, silafluorene−Ph), 7.07 (d, 2H, C=CH), 5.51 (d, 2H, C=CH), 0.60 (s, 6H, CH_3). ^{13}C-{^{1}H} NMR (100.59 MHz, $CDCl_3$): δ 148.5, 147.0, 137.6, 133.5, 130.7, 127.8, 127.1, 126.8, 123.5, 121.2, 111.6, −5.08. ^{29}Si{^{1}H} NMR (99.37 MHz, INEPT, $CDCl_3$, TMS (δ 0.00)) δ −8.8. Calcd for $C_{36}H_{30}Si_2$: C 83.3, H 5.90. Found: C 82.9, H 6.25.

Poly((tetraphenyl)silole−phenylenedivinylene) (4). 1,1-Dihydrido(tetraphenyl)silole (100 mg, 0.26 mmol), 1,4-diethynylbenzene (36 mg, 0.28 mmol), and 0.2 mol % H_2PtCl_6 (**4$_a$**) or 2% Wilkinson's catalyst (**4$_b$**) or 1% Karstedt's catalyst (**4$_c$**) or 1% $Pd(PPh_3)_4$ (**4$_d$**) were vigorously refluxed in toluene (5 mL), under argon for 24 h. The dark orange solution was filtered through a sintered glass frit and evaporated to dryness. The remaining solid was dissolved in 2 mL of THF, and a yellow solid was precipitated with 22 mL of methanol. The precipitation procedure was repeated three times to remove low molecular weight oligomers. A yellow powder was collected by vacuum filtration (69 mg, 51%). Polymer **4$_a$** was used for the detailed characterization. ^{1}H NMR (300.075 MHz,

$CDCl_3$): δ 6.60−7.20 (br, 24H, silole Ph, =CH−Si, and =CH−Ph), 7.40 (br, 4H, phenylene Ph). IR (KBr): $\nu_{C\equiv C,\ Si-H}$ 2142 cm^{-1}, $\nu_{C\equiv C-H}$ 3290 cm^{-1} (acetylinic hydrogen suggests polymer end groups are terminal C≡CH). Calcd for $C_{38}H_{28}Si\cdot 2H_2O$: C 83.2, H 5.88. Found: C 83.2, H 5.80.

Poly(silafluorene−phenylenedivinylene) (5). 1,1-Dihydridosilafluorene (100 mg, 0.55 mmol), 1,4-diethynylbenzene (79 mg, 0.62 mmol), and 0.2 mol % H_2PtCl_6 (**5$_a$**) or 2% Wilkinson's catalyst (**5$_b$**) or 1% Karstedt's catalyst (**5$_c$**) or 1% $Pd(PPh_3)_4$ (**5$_d$**) were stirred at room temperature in toluene (4 mL), under argon for 24 h. The orange solution was filtered and evaporated to dryness. The remaining solid was dissolved in 4 mL of THF and precipitated with 40 mL of methanol. The precipitation procedure was repeated three times to remove low molecular weight oligomers. A white powder was collected by vacuum filtration (122 mg, 68%). Polymer **5$_a$** was used for the detailed characterization. ^{1}H NMR (300.075 MHz, $CDCl_3$): δ 7.20−8.00 (br, 12H, silafluorene H−Ph), 7.00 (br, dd, *trans*-vinyl). IR (KBr): $\nu_{C\equiv C,\ Si-H}$ 2077 cm^{-1} (no C≡CH stretch indicates end groups are terminal Si−H). Calcd for $C_{22}H_{18}Si\cdot H_2O$: C 81.0, H 5.56. Found: C 80.8, H 5.47.

Acknowledgment. This work was supported by the Air Force Office of Scientific Research (AFOSR-MURI# F49620-02-1-0288) and the National Science Foundation (NSF-GRFP). We gratefully acknowledge Dr. Regina Dugan and RedXDefense for providing prints of production-line PETN.

Supporting Information Available: Crystallographic information file (CIF) for compounds **1**−**3** and detailed experimental procedures for the siliptycene (Figure 5). This material is available free of charge via the Internet at http://pubs.acs.org.

References and Notes

(1) Hakansson, K.; Coorey, R. V.; Zubarev, R. A.; Talrose, V. L.; Hakansson, P. *J. Mass Spectrom.* **2000**, *35*, 337−346.
(2) Smith, K. D.; McCord, B. R.; McCrehan, W. A.; Mount, K.; Rowe, W. F. *J. Forensic Sci.* **1999**, *44*, 789−794.
(3) Sylvia, J. M.; Janni, J. A.; Klein, J. D.; Spencer, K. M. *Anal. Chem.* **2000**, *72*, 5834−5840.
(4) Popov, I. A.; Chen, H.; Kharybin, O. N.; Nikolaev, E. N.; Cooks, R. G. *Chem. Commun.* **2005**, *15*, 1953−1955.
(5) Kolla, P. *Anal. Chem.* **1995**, *67*, 184A−189A.
(6) XPRAY Field Test Kit available from Mistral Group, Web URL: http://www.mistralgroup.com/SEC_explosives.asp.
(7) (a) McQuade, D. T.; Pullen, A. E.; Swager, T. M. *Chem. Rev.* **2000**, *100*, 2537−2574. (b) Toal, S. J.; Trogler, W. C. *J. Mater. Chem.* **2006**, *16*, 2871−2883.
(8) La Grone, M.; Cumming, C.; Fisher, M.; Fox, M.; Jacob, S.; Reust, D.; Rockley, M.; Towers, E. www.nomadics.com/EM_aerosense_fluor.pdf (2 Sept 2007).
(9) Seki, K.; Furuyama, T.; Kawasumi, T.; Sakurai, Y.; Ishii, H.; Kajikawa, K.; Ouchi, Y.; Masuda, T. *J. Phys. Chem. B* **1997**, *101*, 9165−9169.
(10) (a) Johansson, D. M.; Theander, M.; Srdanov, G.; Yu, G.; Inganäs, O.; Andersson, M. R. *Macromolecules* **2001**, *34*, 3716−3719. (b) Fan, C.; Plaxico, K. W.; Heeger, A. J. *J. Am. Chem. Soc.* **2002**, *124*, 5642−5643.
(11) Lee, Y.; Liang, Y.; Yu, L. *Synlett* **2006**, *18*, 2879−2893.
(12) (a) Ahn, T.; Song, S.-Y.; Shim, H.-K. *Macromolecules* **2000**, *33*, 6764−6771. (b) Kim, J. K.; Yu, J. W.; Hong, J. M.; Cho, H. N.; Kim, D. Y.; Kim, C. Y. *J. Mater. Chem.* **1999**, *9*, 2171−2176. (c) Kim, J. K.; Hong, S. I.; Cho, H. N.; Kim, D. Y.; Kim, C. Y. *Polym. Bull. (Berlin)* **1997**, *38*, 169−176.
(13) (a) Jin, S. H.; Kang, S. Y.; Kim, M. Y.; Chan, Y. U.; Kim, J. Y.; Lee, K.; Gal, Y. S. *Macromolecules* **2003**, *36*, 3841−3847. (b) Jin, S. H.; Park, H. J.; Kim, J. Y.; Lee, K.; Lee, S. P.; Moon, D. K.; Lee, H. J.; Gal, Y. S. *Macromolecules* **2002**, *35*, 7532−7534.
(14) Grisorio, R.; Mastrorilli, P.; Nobile, C. F.; Romanazzi, G.; Suranna, G. P. *Tetrahedron Lett.* **2005**, *46*, 2555−2558.
(15) Kim, D. S.; Shim, S. C. *J. Polym. Sci., Polym. Chem.* **1999**, *37*, 2263−2273.
(16) Kim, D. S.; Shim, S. C. *J. Polym. Sci., Polym. Chem.* **1999**, *37*, 2933−2940.
(17) Pang, Y.; Ijadi-Maghsoodi, S.; Barton, T. J. *Macromolecules* **1993**, *26*, 5671−5675.
(18) Sumiya, K.-I.; Kwak, G.; Sanda, F.; Masuda, T. *J. Polym. Sci., Polym. Chem.* **2004**, *42*, 2774−2783.
(19) Benfaremo, N.; Sandman, D. J.; Tripathy, S.; Kumar, J.; Yang, K.; Rubner, M. F.; Lyons, C. *Macromolecules* **1998**, *31*, 3595−3599.
(20) Kim, D.-J.; Kim, S.-H.; Zyung, T.; Kim, J.-J.; Cho, I.; Choi, S. K. *Macromolecules* **1996**, *29*, 3657−3660.
(21) Kim, H. K.; Ryu, M.-K.; Kim, K.-D.; Lee, S.-M.; Cho, S.-W.; Park, J.-W. *Macromolecules* **1998**, *31*, 1114−1123.
(22) Rickle, G. K. *J. Appl. Polym. Sci.* **1994**, *51*, 605−612.
(23) Son, D. Y.; Bucca, D.; Keller, T. M. *Tetrahedron Lett.* **1996**, *37*, 1579−1582.
(24) Ohshita, J.; Kunai, A. *Acta Polym.* **1998**, *49*, 379−403.
(25) West, R.; Sohn, H.; Bankwitz, U.; Calabrese, J.; Apeloig, Y.; Mueller, T. *J. Am. Chem. Soc.* **1995**, *117*, 11608−11609.
(26) Yu, G.; Yin, S.; Liu, Y.; Chen, J.; Xu, X.; Sun, X.; Ma, D.; Zhan, X.; Peng, Q.; Shuai, Z.; Tang, B.; Zhu, D.; Fang, W.; Luo, Y. *J. Am. Chem. Soc.* **2005**, *127*, 6335−6346.
(27) Tamao, K.; Uchida, M.; Izumizawa, T.; Kenji, F.; Yamaguchi, S. *J. Am. Chem. Soc.* **1996**, *118*, 11974−11975.
(28) Sohn, H.; Calhoun, R. M.; Sailor, M. J.; Trogler, W. C. *Angew. Chem., Int. Ed.* **2001**, *40*, 2104−2105.
(29) Sohn, H.; Sailor, M. J.; Magde, D.; Trogler, W. C. *J. Am. Chem. Soc.* **2003**, *125*, 3821−3830.
(30) Toal, S. J.; Trogler, W. C. In *Nanotechnology and the Environment*; Karn, B., Masciangioli, T., Zheng, W., Colvin, V., Alivasatos, P., Eds.; Oxford University Press: New York, 2004.
(31) Trogler, W. C. In *Electronic Noses & Sensors for the Detection of Explosives*; Gardner, J. W., Yinon, J., Eds.; Kluwer Academic Publishers: Dordrecht, 2004; p 39.
(32) Toal, S. J.; Sohn, H.; Zakarov, L. N.; Kassel, W. S.; Golen, J. A.; Rheingold, A. L.; Trogler, W. C. *Organometallics* **2005**, *24*, 3081−3087.
(33) Sohn, H.; Huddleston, R. R.; Powell, D. R.; West, R.; Oka, K.; Yonghua, X. *J. Am. Chem. Soc.* **1999**, *121*, 2935−2936.
(34) Sanchez, J. C.; DiPasquale, A. G.; Rheingold, A. L.; Trogler, W. C. *Chem. Mater.*, in press.
(35) Chen, R.-F.; Fan, Q.-L.; Liu, S.-J.; Zhu, R.; Pu, K.-Y.; Huang, W. *Synth. Met.* **2006**, *156*, 1161−1167.
(36) Luo, J.; Xie, Z.; Lam, W. Y. J.; Cheng, L.; Chen, H.; Qiu, C.; Kwok, H. S.; Zhan, X.; Liu, Y.; Zhu, D.; Tang, B. Z. *Chem. Commun.* **2001**, 1740−1741.
(37) Chen, J.; Law, C. C. W.; Lam, J. W. Y.; Dong, Y.; Lo, S. M. F.; Williams, I. D.; Zhu, D.; Tang, B. Z. *Chem. Mater.* **2003**, *15*, 1535−1546.
(38) (a) Moore, D. S. *Rev. Sci. Instrum.* **2004**, *75*, 2499−2512. (b) Singh, S. *J. Hazard. Mater.* **2007**, *144*, 15−28.
(39) Toal, S. J.; Sanchez, J. C.; Dugan, R. E.; Trogler, W. C. *J. Forensic Sci.* **2007**, *52*, 79−83.
(40) Yang, J.-S.; Swager, T. M. *J. Am. Chem. Soc.* **1998**, *120*, 5321−5322.
(41) Ruehlmann, K. *Z. Chem.* **1965**, *5*, 354.
(42) Becker, B.; Corriu, R. J. P.; Henner, B. J. L.; Wojnowski, W.; Peters, K.; von Schnering, H. G. *J. Organomet. Chem.* **1986**, *312*, 305−311.
(43) Chang, L. S.; Corey, J. Y. *Organometallics* **1989**, *8*, 1885−1893.

MA702274C